



The $^{17}\text{O}/^{18}\text{O}$ Ratio of Post-AGB Sources: Canonical and Non-Canonical Populations

Downloaded from: <https://research.chalmers.se>, 2025-01-15 10:46 UTC











Citation for the original published paper (version of record):

Alcolea, J., Masa, E., Khouri, T. et al (2024). The $^{17}\text{O}/^{18}\text{O}$ Ratio of Post-AGB Sources: Canonical and Non-Canonical Populations. *Galaxies*, 12(6). <http://dx.doi.org/10.3390/galaxies12060070>

N.B. When citing this work, cite the original published paper.

Article

The $^{17}\text{O}/^{18}\text{O}$ Ratio of Post-AGB Sources: Canonical and Non-Canonical Populations

Javier Alcolea ^{1,*}, Elisa Masa ¹, Theo Khouri ², Miguel Santander-García ¹, Iván Gallardo Cava ¹, Hans Olofsson ², Carmen Sánchez Contreras ³, Valentín Bujarrabal ¹, Wouter H. T. Vlemmings ² and Daniel Tafoya ²

¹ Observatorio Astronómico Nacional (IGN), C/ Alfonso XII 3 y 5, E-28014 Madrid, Spain; e.masa@oan.es (E.M.); m.santander@oan.es (M.S.-G.); i.gallardocava@oan.es (I.G.C.); v.bujarrabal@oan.es (V.B.)

² Department of Space, Earth and Environment, Chalmers University of Technology, Onsala Space Observatory, 439 92 Onsala, Sweden; theo.khouri@chalmers.se (T.K.); hans.olofsson@chalmers.se (H.O.); wouter.vlemmings@chalmers.se (W.H.T.V.); daniel.tafoya@chalmers.se (D.T.)

³ Centro de Astrobiología (CAB), CSIC-INTA, ESAC Campus, Camino Bajo del Castillo s/n, E-28692 Villanueva de la Cañada, Spain; csanchez@cab.inta-csic.es

* Correspondence: j.alcolea@oan.es

Abstract: Stellar evolution models serve as tools to derive stellar parameters from elemental and isotopic abundance ratios. For low-to-intermediate mass evolved stars, C/O, $^{12}\text{C}/^{13}\text{C}$, and $^{17}\text{O}/^{18}\text{O}$ ratios are proxies of the initial mass, a largely unknown parameter in post-AGB sources, yet fundamental to establish correlations with the main properties of their post-AGB envelopes, progressing in understanding their formation and evolution. In these sources, the C/O ratio can be constrained from the detection of C- or O-bearing species in addition to CO, while the $^{17}\text{O}/^{18}\text{O}$ ratio is straightforwardly determined from the C^{17}O -to- C^{18}O intensity ratio of rotational lines. However, the theory is at odds with the observations. We review the status of the question, including new accurate $^{17}\text{O}/^{18}\text{O}$ ratios for 11 targets (totaling 29). Comparing the results for the $^{17}\text{O}/^{18}\text{O}$ ratios and C-rich/O-rich chemical composition, we find that $\sim 45\%$ of the cases are *canonical*, i.e., the observations align with standard model predictions. O-rich *non-canonical* sources, with $^{17}\text{O}/^{18}\text{O}$ ratios above the expected, can be explained by a premature interruption of their AGB evolution as a consequence of a quasi-explosive ejection of a large fraction of the initial mass. For *non-canonical* C-rich sources, with $^{17}\text{O}/^{18}\text{O}$ ratios below predictions, we suggest the possibility they are extrinsic C-rich stars.

Keywords: AGB and post-AGB evolution; planetary nebulae and pre-planetary nebulae; post-AGB stars; chemical abundances; elemental isotopic ratios; molecular line observations



Citation: Alcolea, J.; Masa, E.; Khouri, T.; Santander-García, M.; Gallardo Cava, I.; Olofsson, H.; Sánchez Contreras, C.; Bujarrabal, V.; Vlemmings, W.H.T.; Tafoya, D. The $^{17}\text{O}/^{18}\text{O}$ Ratio of Post-AGB Sources: Canonical and Non-Canonical Populations. *Galaxies* **2024**, *12*, 70. <https://doi.org/10.3390/galaxies12060070>

Academic Editor: Oleg Malkov

Received: 25 September 2024

Revised: 23 October 2024

Accepted: 23 October 2024

Published: 25 October 2024



Copyright: © 2024 by the authors. Licensee MDPI, Basel, Switzerland. This article is an open access article distributed under the terms and conditions of the Creative Commons Attribution (CC BY) license (<https://creativecommons.org/licenses/by/4.0/>).

1. Elemental and Isotopic Ratios as Proxies of the Initial Stellar Mass in Post-AGB Sources

Low- to intermediate-mass stars (LIMS), with initial masses between 0.8 and $8 M_{\odot}$, are responsible for the enrichment of carbon, nitrogen, and s- and i-process elements of the interstellar medium (ISM), as well as the major producers of cosmic dust. This recycling of matter mostly takes place at the end of LIMS' lives, along the late asymptotic giant branch (late-AGB) and post-AGB phases, when more than one-half of the star's initial mass is thrown back to the ISM via mass loss processes at copious rates [1–4]. During the AGB phase, stars experience gradual chemical changes due to the occurrence of several third dredge-up (TDU) events. All stars enter the AGB phase as O-rich ($\text{C}/\text{O} < 1$), but if the initial mass of the star is in the $\sim 1.5\text{--}4 M_{\odot}$ range, the accumulated effect of the successive TDU events transform them into C-rich ($\text{C}/\text{O} > 1$) by the end of the AGB phase, while also increasing the $^{12}\text{C}/^{13}\text{C}$ ratio [1,3,5,6]. For masses above $4 M_{\odot}$, the hot bottom burning (HBB) process transforms ^{12}C into ^{14}N , thus the stars remain O-rich, with a nitrogen increase in their composition. For masses below $1.5 M_{\odot}$, the small number of TDU

events along the AGB evolution of the star does not produce ^{12}C enrichment enough for the C-rich transformation to occur, the star remaining O-rich. The exact initial mass limits between O-rich, C-rich, and HBB stars depend on the metallicity (see [7] for a review on this topic). The initial mass boundaries between classes given before are valid for the solar metallicities expected in our targets [3,5,7,8]. Because of this ^{12}C enrichment, the $^{12}\text{C}/^{13}\text{C}$ ratio also increases along the AGB evolution, with final values of about 20 and lower for O-rich and HBB stars and larger values of 60 to more than 100 for stars in the C-rich range [5]. In principle, these elemental and isotopic ratios can be used to infer the initial mass of AGB stars; however, as these values change throughout the AGB evolution, this introduces a degree of uncertainty. For example, an O-rich target with a low $^{12}\text{C}/^{13}\text{C}$ may be a star below the transformation limit of $1.5 M_{\odot}$ or a star destined to be C-rich but has not yet evolved far enough through the AGB phase for the ^{12}C -rich transformation to occur. Despite this, several authors have used these ratios to estimate masses for AGB stars [9–12]. Other abundance ratios do not present this problem as they do not vary during the AGB evolution and therefore can be more safely used to derive initial masses. This is the case of the $^{17}\text{O}/^{18}\text{O}$ ratio, which becomes fixed after the first dredge-up (FDU) during the previous red giant phase and remains practically constant along the AGB phase, except for HBB sources where it becomes very large very soon after the beginning of this phase with the occurrence of the second dredge up (SDU) and the destruction of ^{18}O via the $^{18}\text{O}(p,\alpha)^{15}\text{N}$ reaction [5,13]. Since the value of this isotopic ratio also depends on the initial mass, it can potentially be used to weigh LIMS [3,5,14–16]. According to these models, O-rich stars should show $^{17}\text{O}/^{18}\text{O}$ lower than one, while the opposite holds for C-rich sources, with HBB targets lacking ^{18}O [5,16–18].

This problem of not knowing the evolutionary status along the AGB of a target is sorted out if, instead of studying AGB stars, we focus our attention on post-AGB sources. Due to the intense mass loss that characterizes the AGB, LIMS gradually lose their fully convective stellar mantle, leaving the core exposed. At this point, the copious mass loss stops, signaling the end of the AGB phase. From here on, the stars rapidly evolve across the HR diagram, becoming extremely hot in several thousand years. At the same time, their surrounding nebulae, which resulted from the mass loss while on the AGB, also experience drastic changes, ultimately becoming planetary nebulae (PNe) when the central post-AGB source becomes hot enough to photo-dissociate and ionize the molecular gas. As a result of the strong UV radiation of their central stars (CSPNe), PNe are usually poor in molecular content. However, young-PNe (yPNe) and post-AGB nebulae whose central stars are not hot enough to efficiently emit UV photons, in-between objects termed pre-PNe (pPNe), are still rich in molecular gas and therefore are excellent targets to test the stellar mass proxies described before, with the advantage that we already know they have completed their AGB evolution. In these post-AGB sources, the composition of their surrounding nebulae should reflect that of the star at the end of the AGB phase, and in principle, we can safely use all three C/O, $^{12}\text{C}/^{13}\text{C}$, and $^{17}\text{O}/^{18}\text{O}$ ratios to derive the initial mass of the progenitor star, test the consistency of all these three methods and the validity of the standard evolutionary models for these sources: see e.g., [19–22] for $^{12}\text{C}/^{13}\text{C}$ measurements in post-AGBs. Although the number of sources for which these ratios are available in the literature is small, it was soon realized that the theory is at odds with the observations. In addition to sources for which C/O and $^{17}\text{O}/^{18}\text{O}$ ratios suggest similar/compatible initial masses according to standard nucleosynthesis models, which we will denominate *canonical* hereafter, there is a significant number of sources with O-rich chemistry but with $^{17}\text{O}/^{18}\text{O}$ ratios larger than one that would correspond to C-rich stars: see the cases of the *Water Fountains* [23] and M 1–92 [24,25]. Similarly, we also find some chemically C-rich targets with low $^{17}\text{O}/^{18}\text{O}$ ratios typical of O-rich stars: see the case of 89 Her [19]. Given this puzzling situation, we decided to embark on a program to increase the number of targets with precise determination of these chemical and isotopic ratio proxies of the stellar mass, conclude the prevalence of *non-canonical* sources among the post-AGB population, and find out about their possible origin. Southern hemisphere targets are being observed with

ALMA, while northern ones were observed with the IRAM 30 m MRT. Here, we present the results of our IRAM 30 m survey and summarize the status of the question after these and five new sources observed with ALMA [26].

2. Observations and Data Reduction

The new observations presented here were carried out at the 30-m diameter single-dish millimeter radio-telescope (30 m-MRT) operated by the Institut de Radioastronomie Millimétrique¹. This facility is located on the Pico Veleta in Sierra Nevada (Spain) at an altitude of 2850 m. We used the Eight Mixer super-heterodyne Receiver (EMIR), which allows simultaneous observation over a bandwidth of up to 32 GHz. The observations were performed in the dual-band (E090 and E230 receivers at 3 mm and 1.3 mm respectively) single-sideband (LSB) dual-polarization mode (H + V), simultaneously covering two eight-Gigahertz wide frequency ranges, from 86.7 to 93.7 GHz (E090) and from 216.7 to 224.7 GHz (E230), in both polarizations (see Figures 1 and 2). The E230 range covers the $J = 2 - 1$ lines of ^{13}CO , C^{17}O , and C^{18}O for determining the $^{17}\text{O}/^{18}\text{O}$ isotopic ratio. At the same time, the E090 frequencies were selected to cover several molecular lines of HCO^+ , HCN , HNC (and their ^{13}C substitutions), N_2H^+ , SO , and SO_2 to help in distinguishing the C-rich or O-rich nature of the target. The telescope provides a resolving power (HPWB) of $17''$ and $11''$ at 90 and 220 GHz, respectively. This resolution/beamwidth is enough for observing the whole molecular envelope of the targets with the single pointing we performed, except for the cases of NGC 7027, CRL 618, and CRL 2688, where the molecular emitting region is larger than the telescope beam. However, our results on the $^{17}\text{O}/^{18}\text{O}$ ratios and chemical types (C/O-richness) are not affected by the relative sizes of the telescope beam and the target, provided that we use the correct formula for deriving isotopic ratios from line intensity ratios (see Section 3, Equation(1)).

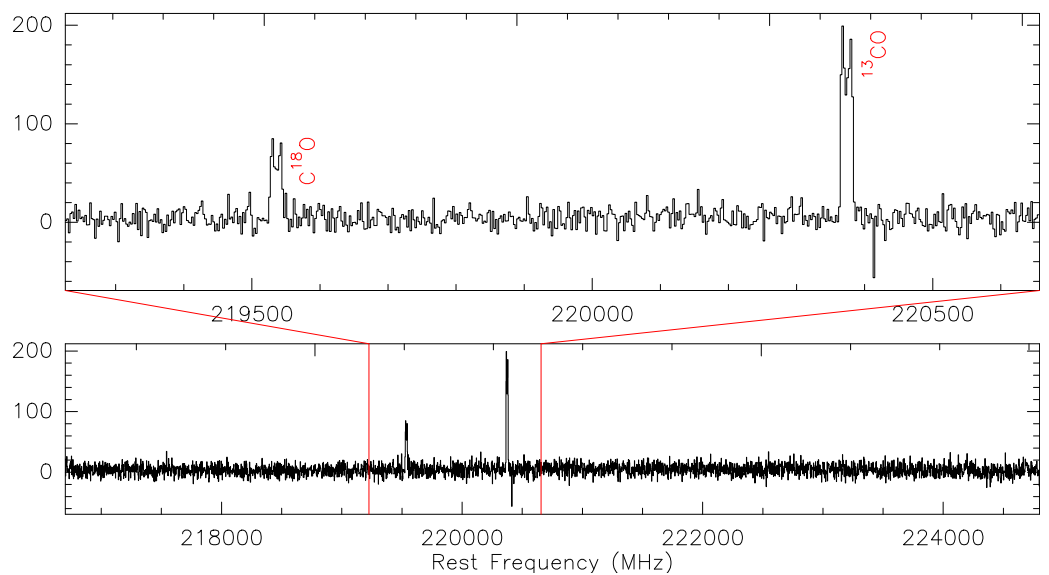


Figure 1. Example of a typical 8 GHz-wide spectrum obtained with the E230 receiver after averaging H and V polarization results for about one hour of telescope time. In the example, the target is the canonical O-rich source IRAS 21282+5050, we have resampled the data to a 3.25 km s^{-1} resolution, and no baseline has been subtracted. The top panel shows a zoom-in view of the indicated ~ 1.4 GHz-wide region of the spectrum. The x -axis is the observed rest frequency for an LSR velocity of -17.5 km s^{-1} ; the y -axis is the T_{mb} intensity in mK. The two lines identified in the spectrum, ^{13}CO and $\text{C}^{18}\text{O } J = 2 - 1$, are indicated.

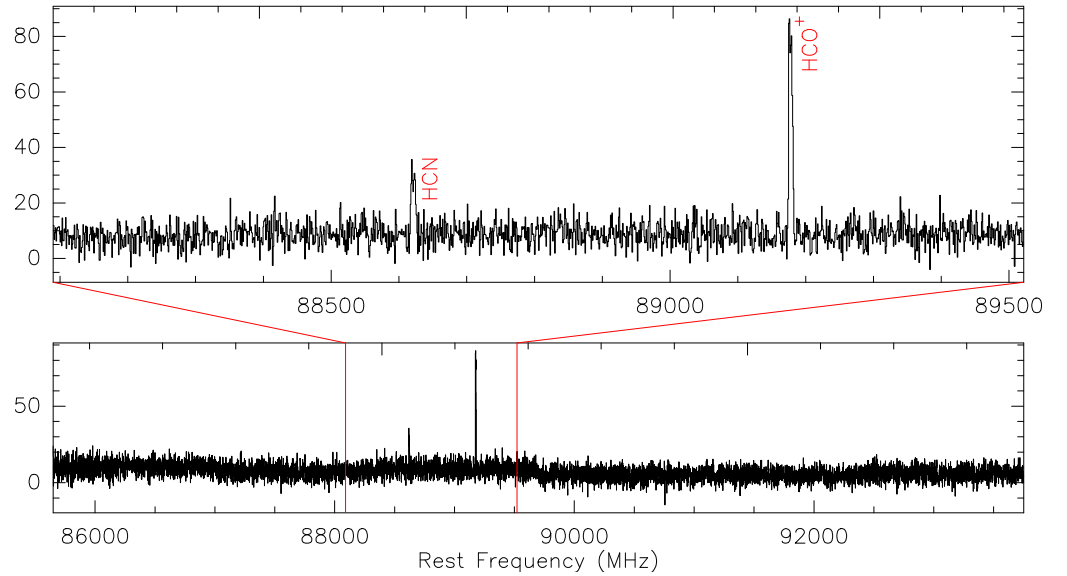


Figure 2. Same as Figure 1 but for the E090 receiver. The two lines identified in the spectrum, HCN and $\text{HCO}^+ J = 1 - 0$, are indicated.

As a spectrometer, we used the fast Fourier transform (FFT) units covering the whole 32 GHz observed ($8 \text{ GHz} \times 2 \text{ receivers} \times 2 \text{ polarizations}$) with a resolution of 200 kHz, equivalent to a velocity resolution of ~ 0.67 and 0.27 km s^{-1} at 90 and 220 GHz, respectively, though the data have been smoothed to a final velocity resolution of 3.25 km s^{-1} for improving the S/N of the spectra. We follow the standard calibration procedure at Pico Veleta, observing hot and cold loads (at ambient and liquid nitrogen temperatures) and the blank sky approximately every 20 min. Hot and cold loads are used to scale spectrometer units into temperature units, while observing the sky brightness provides a measurement of the transmission properties of the local atmosphere via numerical modeling [27]. As a consequence, data from the spectrometer are delivered in (atmosphere-corrected) antenna temperature (T_a^*). The expected absolute calibration accuracy is about 10% for 3 mm data and 15% for 1.3 mm data. However, the relative calibration of the lines simultaneously observed within the same receiver, as in the case of ^{13}CO , C^{17}O , and C^{18}O , is nearly perfect.

The observations were performed by nodding the sub-reflector between the ON-source and OFF-source positions at a frequency of 0.5 Hz (wobbler switching mode, WSW). The OFF-position is acquired at a separation of $\pm 60''$ in azimuth with respect to the target. This procedure ensures an optimal removal of the atmospheric and instrumental contribution to the signal, resulting in very flat baselines in the spectra. The ON–OFF subtractions are accumulated for 4.15 min. This process is repeated three times followed by a calibration of the data. Including overheads, this $3 \times \text{ON–OFF} + \text{Calibration}$ cycle, which was the basic unit of our observing procedure, lasts for 17 min and results in a total effective ON–OFF integration time of 24.7 min (note that we are observing with two receivers, one for each polarization, simultaneously). The telescope’s pointing is good, with typical errors of about $2''$ – $4''$. Nevertheless, pointing was checked, and corrected if necessary, by observing strong continuum sources close in the sky to the science targets. This pointing check was performed when changing to a new target or every two hours, the corrections always being of the same order as the blind pointing accuracy. In any case, these errors have no impact on the relative calibration of the lines observed within the same band.

Data reduction has been performed using the Continuum and Line Analysis Single-dish Software (CLASS) program of the GILDAS² astronomical software package (jul24b version). The process includes data inspection and flagging of bad scans/channels, averaging of valid data, averaging of H and V receivers, smoothing to 3.25 km s^{-1} velocity resolution, removal of residual baselines, and recalibration into T_{mb} (main-beam temperature) scale. Only low-

degree polynomials (usually of zero or first order) have been used for the baseline subtraction. For the conversion of the spectra from T_a^* into T_{mb} scale, we have followed the directions in the EMIR for Astronomers user guide³. As an example of the results, in Figures 1 and 2, we show the full H+V 8 GHz wide spectra for IRAS 21282+5050 after about one hour of telescope time (three basic observing procedure units plus pointing checks).

3. Results

As previously mentioned, we present in detail only the results obtained with the 30 m-MRT; our most recent ALMA results will be thoughtfully presented and discussed in a separate publication [26]. We have observed ten post-AGB sources without previously available $C^{17}O/C^{18}O$ intensity ratios: the pPNe Frosty Leo, IRAS 02229+6808, IRAS 17436+5005, IRAS 19475+3119, IRAS 19500–1709, IRAS 21282+5050, IRAS 22272+5435, IRAS 23304+6147, and IRAS 23321+ 6545, and the PN NGC 6781 (see Table 1). The sources were selected based on their relatively strong ^{13}CO and ^{12}CO emissions in the hope of securing their detection in $C^{17}O$ and $C^{18}O$. We have also re-observed three strong C-rich post-AGB sources (CRL 618, CRL 2688, and NGC 7027) to obtain $C^{17}O/C^{18}O$ intensity ratios consistently. Finally, we have also included two control targets, the S-type AGB star CRL 2477 and the post-red supergiant AFGL 2343. We have detected both $C^{17}O$ and $C^{18}O$ $J = 2 - 1$ in all targets but two: IRAS 19475+3119 and NGC 6781. Based on the detected species other than CO, we have also determined the C-rich or O-rich nature of our targets in all cases but IRAS 19475+3119, where only ^{13}CO was detected. Therefore, we provide for the first time or improve $C^{17}O/C^{18}O$ for 11 post-AGB sources (about 1/3 of all sources for which this ratio has been determined), also including a chemical classification based on the molecular composition of their envelopes.

Table 1. Species other than ^{13}CO detected in our IRAM 30-m MRT survey of post-AGB sources.

Source Name	Species Detected	Chemical Type
Frosty Leo ¹	$C^{17}O$, $C^{18}O$, SiO, ^{29}SiO , SO, SO ₂ , H ₂ S, HCN	O-rich
IRAS 02229+6808 ¹	$C^{17}O$, $C^{18}O$, SiO, ^{13}CS , SiS, SiC ₂ , HCN, H ¹³ CN, HNC, HC ₃ N, HC ₅ N, ^{13}CN , C ₃ N, CH ₃ CN, C ₂ H, C ₄ H	C-rich
IRAS 17436+5005 ¹	$C^{17}O$, $C^{18}O$, SiO	O-rich
IRAS 19475+3119 ¹		unknown
IRAS 19500–1709 ¹	$C^{17}O$, $C^{18}O$, HCN	C-rich
IRAS 21282+5050 ¹	$C^{17}O$, $C^{18}O$, HCN, HCO ⁺	C-rich
IRAS 22272+5435 ¹	$C^{17}O$, $C^{18}O$, ^{28}SiO , ^{13}CS , SiC ₂ , HCN, H ¹³ CN, HNC, HC ₃ N, HC ₅ N, HN ¹³ C, HCO ⁺ , C ₂ H, C ₄ H, C ₃ N	C-rich
IRAS 23304+6147 ¹	$C^{17}O$, $C^{18}O$, SiC ₂ , HCN, H ¹³ CN, HNC, HC ₃ N, HC ₅ N, ^{13}CN , C ₂ H, C ₄ H, C ₃ N	C-rich
IRAS 23321+6545 ¹	$C^{17}O$, $C^{18}O$, SiS, SiC ₂ , HCN, H ¹³ CN, HNC, HC ₃ N, CH ₃ CN	C-rich
NGC 6781 ²	HCN, HCO ⁺ , HNC	C-rich
CRL 618 ¹	$C^{17}O$, $C^{18}O$, SiS, SiC ₂ , HCN, H ¹³ CN, HCO ⁺ , H ¹³ CO ⁺ , HNC, HN ¹³ C, ^{13}CN , HC ₃ N, HC ₅ N, HC ₇ N, CH ₃ CN, C ₃ N, etc.	C-rich
CRL 2688 ¹	$C^{17}O$, $C^{18}O$, SiO, SiS, SiC ₂ , HCN, H ¹³ CN, HCO ⁺ , HNC, HN ¹³ C, C ₂ H, C ₄ H, HC ₃ N, HC ₅ N, ^{13}CS , ^{13}CN , NaCN, <i>c</i> -C ₃ H ₂	C-rich
NGC 7027 ²	$C^{17}O$, $C^{18}O$, HCN, H ¹³ CN, HNC, <i>c</i> -C ₃ H ₂ , N ₂ H ⁺ , HCO ⁺ , H ¹³ CO ⁺ , HC ¹⁷ O ⁺ , HC ¹⁸ O ⁺ , etc.	C-rich

Table 1. Cont.

Source Name	Species Detected	Chemical Type
CRL 2777 ³	C ¹⁷ O, C ¹⁸ O, SiO, SiS, SiC ₂ , ¹³ CS, HCN, H ¹³ CN, HNC, HN ¹³ C, C ₂ H, C ₄ H, HC ₃ N, HC ₅ N	C-rich
AFGL 2324 ⁴	C ¹⁷ O, C ¹⁸ O, SiO, ²⁹ SiO, HCN, SO, H ₂ S	O-rich

¹ post-AGB: pPN. ² post-AGB: PN. ³ S-type AGB star: control target. ⁴ post-red super giant: control target.

The C/O ratio is not determined but constrained to be higher or lower than one, i.e., whether the source is C-rich (C/O > 1) or O-rich (C/O < 1), based on the detected species other than CO. In addition to H₂, the molecular content of AGB and post-AGB envelopes is largely dominated by CO. This creates a clear dichotomy in the inventory of the other species detected, with a prevalence of C-bearing species in C-rich sources, such as CS, HC_{2n+1}N, C_{2n}H, SiC₂, and other complex organic molecules, and of O-bearing species in O-rich sources, such as SiO, SO, SO₂, H₂O, and OH ([28,29] and references therein). Some molecules are unique to each of the two chemical types like SO₂ and SiC₂, while in other cases, as for SiO, CS, HCN, etc., it is their relative strength that informs us about the chemical nature of the object. We summarize the non-CO detected species in each source and the assigned chemical type depending solely on these detections in Table 1. As can be seen, our sample comprises three O-rich sources and 11 C-rich sources (including the three targets re-observed and the control sources). In Figure 3, we show an example of some of the lines identified in the *non-canonical* C-rich pPN IRAS 22272+5435. Note the strong HCN line, that SiS is more intense than SiO, and that SO remains undetected. In addition, we have also identified lines of ¹³CS, SiC₂, HC₃N, HC₅N, C₂H, C₄H, and C₃N, indicating that the object is C-rich. However, C¹⁸O is notably stronger than C¹⁷O, an unexpected result for a C-rich envelope.

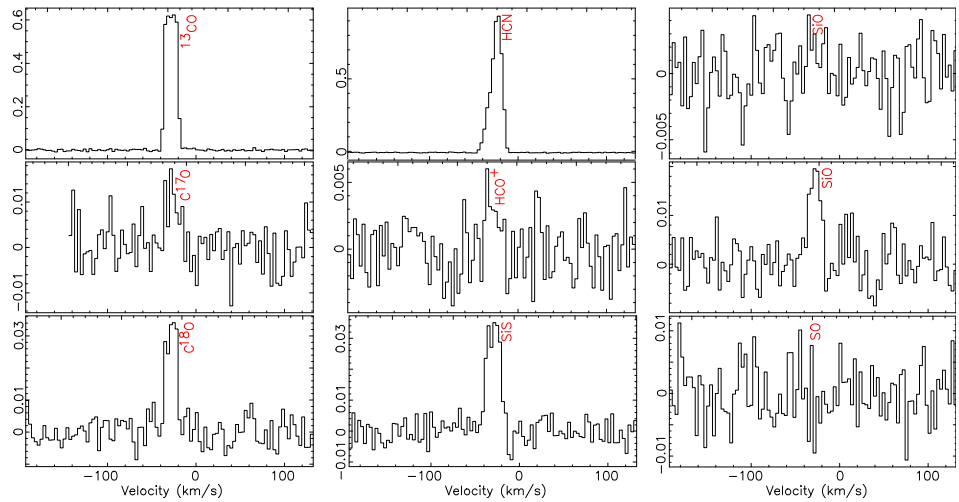


Figure 3. Spectra of some of the lines detected in the C-rich *non-canonical* pPN IRAS 22272+5435. All intensities are given in K in T_{mb} temperature scale. The x -axis is the observed velocity with respect to the Local Standard of Rest.

In contrast, the ¹⁷O/¹⁸O ratio has been determined from the intensity ratio of the $J = 2 - 1$ rotational lines of the corresponding oxygen substitutions of CO. Assuming that these lines are optically thin, have similar excitation, and also identical extent, something that is very reasonable and has been confirmed where accurately measured [24,25], the C¹⁷O/C¹⁸O abundance ratio is given by the expression [16,23,26]

$$\frac{C^{17}O}{C^{18}O} = \frac{I(C^{17}O J = 2 - 1)}{I(C^{18}O J = 2 - 1)} \times \frac{A_{ij}(C^{18}O J = 2 - 1) \nu(C^{18}O J = 2 - 1)}{A_{ij}(C^{17}O J = 2 - 1) \nu(C^{17}O J = 2 - 1)} \times \frac{\Omega(C^{18}O J = 2 - 1)}{\Omega(C^{17}O J = 2 - 1)}. \quad (1)$$

In this expression, I , A_{ij} , and ν are the integrated intensity, Einstein-A coefficient, and frequency of the corresponding rotational line, respectively. The Einstein-A coefficient and line frequency ratios are 0.941 and 0.977, respectively. The factor $\Omega(\text{C}^{18}\text{O } J = 2 - 1)/\Omega(\text{C}^{17}\text{O } J = 2 - 1)$ corrects for the different source-to-beam size ratios of the different lines. Its value is 1 in the case that the source is larger than the beam (as for CRL 618, CRL 2688, and NGC 7027), and $\nu(\text{C}^{18}\text{O } J = 2 - 1)/\nu(\text{C}^{17}\text{O } J = 2 - 1) = 0.977$ if the source is not resolved (the rest of the cases). Assuming that there is no chemical fractionation either, the $^{17}\text{O}/^{18}\text{O}$ ratio results in

$$\frac{^{17}\text{O}}{^{18}\text{O}} \approx \frac{\text{C}^{17}\text{O}}{\text{C}^{18}\text{O}} = \frac{I(\text{C}^{17}\text{O } J = 2 - 1)}{I(\text{C}^{18}\text{O } J = 2 - 1)} \times \Gamma, \quad (2)$$

where Γ is the product of the Einstein-A coefficient, line frequency, and source-to-beam size ratios, with a value of 0.92 or 0.90 depending on whether the source is resolved or not. Note that the difference between the two values is rather small, only 2.3%, which is negligible in the unlikely event of using the value for an unresolved object for an extended source and vice versa.

Our new values for $^{17}\text{O}/^{18}\text{O}$ ratios are summarized in Figure 4. Here, we also plot 18 additional sources for which we know their chemical composition and $^{17}\text{O}/^{18}\text{O}$ ratios estimated following a similar procedure. Here, the y -position of each source reflects the actual value of the $^{17}\text{O}/^{18}\text{O}$ ratio, while the x -position just indicates whether the source is O-rich, C-rich, or an HBB source. The white line marks the expected value for the $^{17}\text{O}/^{18}\text{O}$ abundance ratio as a function of the initial stellar mass (x -axis) according to standard evolution models for solar metallicities ([3,16,30,31] and references therein). Note that the C/O ratio has not been numerically computed; we only know whether the star/envelope is C-rich or O-rich by the molecular species other than CO detected in the source.

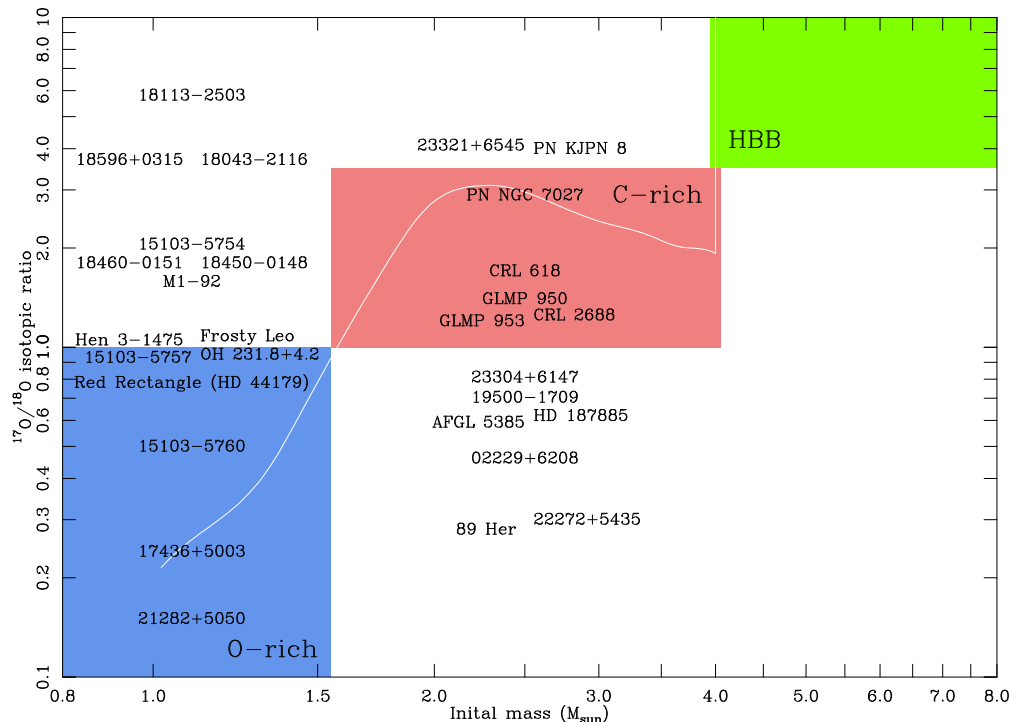


Figure 4. Status of the C/O (obtained from the chemical composition of the envelopes) and $^{17}\text{O}/^{18}\text{O}$ (from C^{17}O and C^{18}O measurements) ratios in post-AGB sources (pPNe and young-PNe). In this $^{17}\text{O}/^{18}\text{O}$ vs. initial mass (in M_{\odot}) plot: the y -position of the labels indicates the measured value of the

$^{17}\text{O}/^{18}\text{O}$ ratio; the x -position reflects the observed chemistry of the envelopes (O-rich, C-rich, or HBB-sources). The white line indicates the predictions of solar metallicity standard models for the surface value of $^{17}\text{O}/^{18}\text{O}$ at the end of the AGB phase as a function of the stellar initial mass: we have taken an average value of predictions from STARS, FRANEC, and Stromlo/Monash codes (see [5,16,30,31] and the references therein). Stars within the colored boxes (and slightly above for C-stars) are *canonical* as they agree with model predictions. Sources lying outside these boxes, 16 out of 29, are *non-canonical*, indicating a non-standard AGB evolution. See text for further details. Names such as NNNNN \pm NNNN are short forms of IRAS NNNNN \pm NNNN. $^{17}\text{O}/^{18}\text{O}$ values for Frosty Leo, IRAS 02229+6808, IRAS 17436+5005, IRAS 19500–1709, IRAS 21282+5050, IRAS 22272+5435, IRAS 23304+6147, IRAS 23321+6545, CRL 618, CRL 2688, and PN NGC 7027 are from this work; values for the Red Rectangle (HD 44179) and 89 Her are from [19]; value for OH 231.8+4.2 is from [32]; values for IRAS 15103–5754, IRAS 15103–5757, IRAS 15103–5757, IRAS 18043–2116, IRAS 18113–2503, IRAS 18450–0148, IRAS 18460–0151, and IRAS 18596+0315 are from [23]; value for M1–92 is from [24,26]; values for AFGL 5385, Hen 3–1475, HD 187885, GLMP 950, and GLMP 953 are from [26]; and value for PN KJPN 8 is from [33].

4. Discussion: The Canonical and Non-Canonical Post-AGB Populations

The first result is that we do not find any source in the range of 4 to 8 M_{\odot} , whereas, as a result of the HBB process, the stars retain their O>C initial composition and $^{17}\text{O}/^{18}\text{O}$ become very large due to the destruction of ^{18}O . For O-rich sources, with initial masses between 1 and 1.5 M_{\odot} , we find six sources with $^{17}\text{O}/^{18}\text{O}$ ratios $\lesssim 1$, that are compatible with model predictions (*canonical* sources). However, there are nine (*non-canonical*) sources for which their $^{17}\text{O}/^{18}\text{O}$ ratios are larger one, which corresponds to C-rich stars. For the C-rich sources, with expected masses between 1.5 and 4 M_{\odot} , a similar situation is observed: we have seven *canonical* sources with $^{17}\text{O}/^{18}\text{O} > 1$ consistent with predictions, and an equal number of (*non-canonical*) sources with $^{17}\text{O}/^{18}\text{O}$ values < 1 expected for O-rich sources. In summary, we have fewer well-behaved sources (13 cases, which represents $\sim 45\%$ of the whole sample) than oddballs (16, $\sim 55\%$).

Non-canonical O-rich sources, with $^{17}\text{O}/^{18}\text{O} > 1$, are interpreted as a result of an interrupted AGB evolution of stars that were bound to be C-rich. Since for stars with initial masses between 1.5 and 4 M_{\odot} the C/O ratio increases along the AGB evolution, it may happen that if this evolution is interrupted the star remains O-rich. This hypothesis is in line with the belief that some post-AGB nebulae are the result of a sudden ejection of mass (possibly as a consequence of merging with a companion, for example) that terminates the AGB evolution early [34,35]. This scenario has been proposed to explain the formation of the O-rich pPN M1–92, for which we obtain a $^{17}\text{O}/^{18}\text{O}$ ratio of 1.6 that corresponds to an initial mass of 1.7 M_{\odot} , and that should have been turned C-rich by the end of the AGB if the star had completed this phase [24,25]. This idea is further supported by our recent finding of a $^{12}\text{C}/^{13}\text{C}$ ratio ≈ 30 in M1–92, which lies in between those expected at the beginning (≈ 20) and end (≈ 70) of the AGB phase for a 1.7 M_{\odot} star [24]. Most likely, the premature end of this phase resulted in a lower than expected ^{12}C enrichment and, as a consequence, a C/O < 1 along with a moderate value for the $^{12}\text{C}/^{13}\text{C}$ ratio. As for the *non-canonical* C-rich sources, there is no clear working hypothesis, but given the bipolar (and therefore probably binary) nature of the sources, we suggest that they could be the result of mass transfer phenomena such as those occurring in extrinsic carbon stars [36], but see also the work by [14].

Author Contributions: Conceptualization, J.A., T.K., M.S.-G., H.O., C.S.C., V.B., W.H.T.V. and D.T.; methodology, J.A., T.K., M.S.-G., H.O., C.S.C., V.B. and W.H.T.V.; software, J.A. and T.K.; validation, J.A. and T.K.; formal analysis, J.A., E.M., I.G.C. and T.K.; investigation, J.A., E.M., T.K., M.S.-G., I.G.C., H.O., C.S.C., V.B., W.H.T.V. and D.T.; resources, J.A., E.M., I.G.C. and T.K.; data curation, J.A., E.M., I.G.C. and T.K.; writing—original draft preparation, J.A., T.K., M.S.-G., I.G.C. and H.O.; writing—review and editing, J.A., E.M., T.K., M.S.-G., I.G.C., H.O., C.S.C., V.B., W.H.T.V. and D.T.; visualization, J.A. and T.K.; supervision, J.A., T.K., H.O. and C.S.C.; project administration, J.A. and

C.S.C.; funding acquisition, J.A., V.B. and C.S.C. All authors have read and agreed to the published version of the manuscript.

Funding: This research is part of the I+D+i projects PID 2019–105203GB–C21 and 2019–105203GB–C22 funded by Spanish AEI (MICIU) grant 10.13039/501100011033 <http://doi.org/10.13039/501100011033> (accessed on 24 October 2024).

Data Availability Statement: The raw data supporting the conclusions of this article will be made available by the authors on request.

Conflicts of Interest: The authors declare no conflicts of interest.

Notes

- ¹ IRAM is an international research institute. Founded in 1979, it is participated in by the French *Centre National de la Recherche Scientifique* (CNRS), the German *Max-Planck-Gesellschaft* (MG), and the Spanish *Instituto Geográfico Nacional* (IGN) through the *Observatorio Astronómico Nacional* (OAN). IRAM operates the single-dish 30m-MRT in Spain and the NOEMA interferometer in the French Alps.
- ² GILDAS is a collection of state-of-the-art software oriented toward (sub-)millimeter radio-astronomical applications (either single-dish or interferometric). The GILDAS developments are supported by IPAG (*Observatoire de Grenoble*) and IRAM, with additional contributions from LAB (*Observatoire de Bordeaux*) and LERMA (*Observatoire de Paris*). For more information, see <https://www.iram.fr/IRAMFR/GILDAS> (accessed on 24 September 2024).
- ³ EMIR relevant information can be found at <https://publicwiki.iram.es/EmirforAstronomers> (accessed on 24 September 2024).

References

1. Herwig, F. Evolution of Asymptotic Giant Branch Stars. *Annu. Rev. Astron. Astrophys.* **2005**, *43*, 435. [[CrossRef](#)]
2. Höfner, S.; Olofsson, H. Mass loss of stars on the asymptotic giant branch. Mechanisms, models and measurements. *Astron. Astrophys. Rev.* **2018**, *R26*, 1H. [[CrossRef](#)]
3. Karakas, A.I. Helium enrichment and carbon-star production in metal-rich populations. *Mon. Not. R. Astron. Soc.* **2014**, *445*, 347. [[CrossRef](#)]
4. Vassiliadis, E.; Wood, P.R. Evolution of Low- and Intermediate-Mass Stars to the End of the Asymptotic Giant Branch with Mass Loss. *Astrophys. J.* **1993**, *413*, 641. [[CrossRef](#)]
5. Karakas, A.I.; Lugaro, M. Stellar Yields from Metal-rich Asymptotic Giant Branch Models. *Astrophys. J.* **2016**, *826*, 26K. [[CrossRef](#)]
6. Ventura, P.; D’Antona, F. Full computation of massive AGB evolution. I. The large impact of convection on nucleosynthesis. *Astron. Astrophys.* **2005**, *431*, 279. [[CrossRef](#)]
7. Straniero, O.; Abia, C.; Domínguez, I. The carbon star mystery: 40 years later: Theory and observations. *Eur. Phys. J. A* **2023**, *59*, 17S. [[CrossRef](#)]
8. Straniero, O.; Gallino, R.; Cristallo, S. s process in low-mass asymptotic giant branch stars. *Nuc. Phys. A* **2006**, *777*, 311. [[CrossRef](#)]
9. Abia, C.; Isern, J. ¹²C/¹³C ratios and Li abundances in C stars: Evidence for deep mixing? *Mon. Not. R. Astron. Soc.* **1997**, *289*, L11A. [[CrossRef](#)]
10. Ramstedt, S.; Olofsson, H. The ¹²CO/¹³CO ratio in AGB stars of different chemical type. Connection to the ¹²C/¹³C ratio and the evolution along the AGB. *Astron. Astrophys.* **2014**, *566*, A145R. [[CrossRef](#)]
11. Schöier, F.L.; Olofsson, H. The ¹²C/¹³C-ratio in cool carbon stars. *Astron. Astrophys.* **2000**, *359*, 586S.
12. Wallerstein, G.; Balick, B.; Alcolea, J.; Bujarrabal, V.; Vanture, A.D. Carbon isotopic abundance ratios in S-type stars. *Astron. Astrophys.* **2011**, *535*, A101W. [[CrossRef](#)]
13. Lattanzio, J.; Frost, C.; Cannon, R.; Wood, P.R. Hot bottom burning in intermediate mass stars. *Mem. Della Soc. Astron. Ital.* **1996**, *67*, 729L.
14. Abia, C.; Hedrosa, R.P.; Domínguez, I.; Straniero, O. The puzzle of the CNO isotope ratios in asymptotic giant branch carbon stars. *Astron. Astrophys.* **2017**, *599*, 9A. [[CrossRef](#)]
15. Boothroyd, A.I.; Sackmann, I.J. The CNO Isotopes: Deep Circulation in Red Giants and First and Second Dredge-up. *Astrophys. J.* **1999**, *510*, 232. [[CrossRef](#)]
16. De Nutte, R.; Decin, L.; Olofsson, H.; Lombaert, R.; de Koter, A.; Karakas, A.; Milam, S.; Ramstedt, S.; Stancliffe, R.J.; Homan, W.; Van de Sande, M. Nucleosynthesis in AGB stars traced by oxygen isotopic ratios. I. Determining the stellar initial mass by means of the ¹⁷O/¹⁸O ratio. *Astron. Astrophys.* **2017**, *600*, A71. [[CrossRef](#)]
17. Justtanont, K.; Teysier, D.; Barlow, M.J.; Matsuura, M.; Swinyard, B.; Waters, L.B.F.M.; Yates, J. OH/IR stars and their superwinds as observed by the Herschel Space Observatory. *Astron. Astrophys.* **2013**, *556*, 101J. [[CrossRef](#)]
18. Justtanont, K.; Barlow, M.J.; Blommaert, J.A.D.L.; Decin, L.; Kerschbaum, F.; Matsuura, M.; Olofsson, H.; Swinyard, B.; Teysier, D.; Waters, L.B.F.M.; et al. H₂O Isotopologues in Extreme OH/IR Stars. *Astron. Astrophys.* **2015**, *578*, 115J. [[CrossRef](#)]
19. Gallardo Cava, I.; Bujarrabal, V.; Alcolea, J.; Gómez-Garrido, M.; Santander-García, M. Chemistry of nebulae around binary post-AGB stars: A molecular survey of mm-wave lines. *Astron. Astrophys.* **2022**, *659*, A134G. [[CrossRef](#)]
20. Balser, D.S.; McMullin, J.P.; Wilson, T.L. CO Isotopes in Planetary Nebulae. *Astrophys. J.* **2002**, *572*, 326B. [[CrossRef](#)]

21. Palla, F.; Bachiller, R.; Stanghellini, L.; Tosi, M.; Galli, D. Measurements of $^{12}\text{C}/^{13}\text{C}$ in planetary nebulae: Implications on stellar and Galactic chemical evolution. *Astron. Astrophys.* **2000**, *355*, 69P.
22. Sánchez Contreras, C.; Sahai, R. OPACOS: OVRO Post-AGB CO (1-0) Emission Survey. I. Data and Derived Nebular Parameters. *Astrophys. J.* **2012**, *S203*, 16S. [[CrossRef](#)]
23. Khouri, T.; Vlemmings, W.H.T.; Tafuya, D.; Pérez-Sánchez, A.F.; Sánchez Contreras, C.; Gómez, J.F.; Imai, H.; Sahai, R. Observational identification of a sample of likely recent common-envelope events. *Nat. Astron.* **2022**, *6*, 275. [[CrossRef](#)]
24. Masa, E.; Alcolea, J.; Santander-García, M.; Bujarrabal, V.; Sánchez Contreras, C.; Castro-Carrizo, A. M 1-92: The Death of an AGB Star Told by Its Isotopic Ratios. *Galaxies* **2024**, *12*, 63. [[CrossRef](#)]
25. Alcolea, J.; Agúndez, M.; Bujarrabal, V.; Castro-Carrizo, A.; Desmurs, J.-F.; Sánchez Contreras, C.; Santander-García, M. M 1-92 revisited: The chemistry of a common envelope nebula? In *Why Galaxies Care About AGB Stars: A Continuing Challenge Through Cosmic Time*; Proceedings of the International Astronomical Union; Cambridge University Press: Cambridge, UK, 2019; Volume 343, p. 343A.
26. Khouri, T.; Tafuya, D.; Vlemmings, W.H.T.; Olofsson, H.; Sánchez Contreras, C.; Alcolea, J.; Gómez, J.F.; Velilla-Prieto, L.; Sahai, R.; Santander-García, M.; et al. ALMA observations of CO isotopologues towards six obscured post-AGB stars. *Astron. Astrophys.* **2024**, *submitted*.
27. Pardo, J.R.; Serabyn, E.; Cernicharo, J. Atmospheric transmission at microwaves (ATM): An improved model for millimeter/submillimeter applications. *IEEE Trans. Antennas Propag.* **2001**, *49*, 1683. [[CrossRef](#)]
28. Bujarrabal, V.; Fuente, A.; Omont, A. Molecular observations of O- and C-rich circumstellar envelopes. *Astron. Astrophys.* **1994**, *285*, 247B.
29. Bujarrabal, V.; Fuente, A.; Omont, A. The Discrimination between O- and C-rich Circumstellar Envelopes from Molecular Observations. *Astrophys. J.* **1994**, *421*, L47B. [[CrossRef](#)]
30. Cristallo, S.; Piersanti, L.; Straniero, O.; Gallino, R.; Domínguez, I.; Abia, C.; Di Rico, G.; Quintini, M.; Bisterzo, S. Evolution, Nucleosynthesis, and Yields of Low-mass Asymptotic Giant Branch Stars at Different Metallicities. II. The FRUITY Database. *Astrophys. J.* **2011**, *S197*, 17C. [[CrossRef](#)]
31. Stancliffe, R.J.; Eldridge, J.J. Modelling the binary progenitor of Supernova 1993J. *Mon. Not. R. Astron. Soc.* **2009**, *396*, 1699S. [[CrossRef](#)]
32. Sánchez Contreras, C.; Velilla, L.; Alcolea, J.; Quintana-Lacaci, G.; Cernicharo, J.; Agúndez, M.; Teyssier, D.; Bujarrabal, V.; Castro-Carrizo, A.; Daniel, F.; et al. mm-wave and far-IR Molecular line survey of OH 231.8+4.2: Hard-boiled rotten eggs. In *Asymmetrical Planetary Nebulae VI Conference; Proceedings of the Conference, Riviera Maya, Mexico, 4–8 November 2013*; Morisset, C., Delgado-Inglada, G., Torres-Peimbert, S., Eds.; 2013; p. 88S. Available online: <http://www.astroscu.unam.mx/apn6/PROCEEDINGS/> (accessed on 24 September 2024).
33. Velilla-Prieto, L.; Vlemmings, W.H.T.; Olofsson, H.; del Rey, R.; Khouri, T.; Castro-Carrizo, A.; Bujarrabal, V.; Alcolea, J.; Agúndez, M.; Saberi, M. Molecular gas after the AGB: The cases of V Hydrae and KJPN 8. *Galaxies* **2024**, *submitted*.
34. Alcolea, J.; Neri, R.; Bujarrabal, V. Minkowski's footprint revisited. Planetary nebula formation from a single sudden event? *Astron. Astrophys.* **2007**, *468*, L41A. [[CrossRef](#)]
35. Blackman, E.G.; Lucchini, S. Using kinematic properties of pre-planetary nebulae to constrain engine paradigms. *Mon. Not. R. Astron. Soc.* **2014**, *440*, L16B. [[CrossRef](#)]
36. Foster, S.; Schiavon, R.P.; de Castro, D.B.; Lucatello, S.; Daher, C.; Penoyre, Z.; Price-Whelan, A.; Badenes, C.; Fernández-Trincado, J.G.; García-Hernández, D.A.; et al. Carbon enrichment in APOGEE disk stars as evidence of mass transfer in binaries. *Astron. Astrophys.* **2024**, *689*, A230F. [[CrossRef](#)]

Disclaimer/Publisher's Note: The statements, opinions and data contained in all publications are solely those of the individual author(s) and contributor(s) and not of MDPI and/or the editor(s). MDPI and/or the editor(s) disclaim responsibility for any injury to people or property resulting from any ideas, methods, instructions or products referred to in the content.